RSC Advances

ROYAL SOCIETY OF CHEMISTRY

www.rsc.org/advances

Controllable synthesis of high quality monolayer WS_2 on SiO_2/Si substrate by chemical vapor deposition

Qi Fu,[a] Wenhui Wang,[a] Lei Yang,[a] Jian Huang,[a] Jingyu Zhang,[c] Bin Xiang*[a,b]

[a]Department of Materials Science & Engineering, CAS key Lab of Materials for Energy Conversion, University of Science and Technology of China, Hefei, Anhui, 230026, China.

* E-mail: binxiang@ustc.edu.cn

[b]Synergetic Innovation Center of Quantum Information & Quantum Physics, University of Science and Technology of China, Hefei, Anhui 230026, China

[c]Molecular Foundry, Lawrence Berkeley National Laboratory, 1 Cyclotron Rd, Berkeley, CA 94720, USA

Abstract

Tungsten disulfide (WS_2), with transformation from indirect to direct band transitions when scaled down to monolayer, exhibits great potential in future micro-device applications. In this work, we report a controllable route for monolayer WS_2 synthesis. The high-quality of as-grown monolayer WS_2 was confirmed by optical microscopy, atomic force microscopy (AFM), high resolution scanning transmission electron microscopy (HRSTEM), Raman spectroscopy, and photoluminescence (PL). The impacts of growth parameters (including gas flow rate and reaction temperature) on the morphology of WS_2 domain were investigated. A growth mechanism is proposed based on the experimental analysis. Our results also provide some general guidelines for other two dimensional (2D) monolayer synthesis of transition metal dichalcogenides (TMD).

Introduction

The research on graphene in the past decades[1-3] has raised great interest in both fundamental science and industrial aspects for next-generation.[4-6] However, with a zero energy band gap, graphene is considered ill-fitted to many applications, i.e. field effect transistors. The layered transition metal dichalcogenides (TMD)[7-11] such as MoS_2, WS_2, WSe_2, has attracted considerable attention because of their special semiconductor properties. An indirect band gap in TMD materials can be switched into a direct band gap when scaled down from bulk to monolayer.[12, 13] The emergence of these 2D materials provides grand possibilities for future semiconductor devices, for instance photovoltaic and photocatalytic applications.[14]

So far, the studies on MoS_2 monolayer have been fruitful: the mature growth condition,[15-18] the impressive electronic and optical properties,[19-22] the great application potential in 2D semiconductors,[23-26] etc. Similar to MoS_2, the layered structure of WS_2 is formed by sandwiching one layer of W atoms into two layers of S atoms.[27] The monolayer WS_2 possesses a direct energy gap of ~2 eV,[19] bringing out extensive enhancement of visible light emission, as proved in previous studies.[28] The strong spin-orbit coupling and the splitting of valence bands at K/K' points in the Brillouin zone with a sub-gap of around 0.4 eV were also observed in monolayer WS_2.[29] All these interesting properties indicate WS_2 as a promising candidate for valleytronics, optoelectronics, nanoelectronics and spintronics[30] in the next decades. Mechanical exfoliation,[13, 19] chemical exfoliation[29, 31] and chemical vapor deposition (CVD)[28, 32, 33] have been applied to obtain WS_2 domains. Among these methods,

chemical vapor deposition is considered the most promising one to meet the requirement of nanodevice fabrication, for its superiority in guarantee of high crystalline quality, large domain size, and well-controlled thickness. Monolayer WS_2 has been successfully synthesized using CVD method by several research groups.[28,32,33] However, among those reported work, the growth parameters for the monolayer WS_2 growth are greatly distinct from each other. For instance, by utilizing the WO_3 powder and S powder, Cong et al. reports that monolayer WS_2 can be grown at 750°C by flowing 100 sccm carrier gas, while Lee et al. reports that monolayer WS_2 can be grown at 800 °C by flowing 5 sccm carrier gas. It raises our interest in what effects on the monolayer WS_2 synthesis those growth parameters exert? In our paper, we report systematic studies of the growth parameter effects on monolayer WS_2 synthesis. It reveals that the growth temperature and gas flow rate play key roles on monolayer WS_2 nucleation and growth, determining the size of the WS_2 domains. Our results enable us to the realization of controllable monolayer WS_2 growth, and also provide some general guidelines for other 2D material growth.

Here, we report a controllable synthesis of large-area high quality of monolayer WS_2 triangular domains on SiO_2/Si wafer via sulfurization of WO_3 powder with argon and H_2 (3%) mixed carrier gas in a two-temperature zone furnace, by atmospheric pressure chemical vapor deposition (APCVD) method. Atomic force microscopy (AFM), high resolution scanning transmission electron microscopy (HRSTEM), Raman spectroscopy, and photoluminescence (PL) were utilized to characterize the as-growth monolayer WS_2. To probe the effects of growth parameters and growth

mechanism, we systematically studied the growth parameters, i.e., flow rate of carrier gas and growth temperature.

Experiment details

The experiment was proceeded in a two-temperature zone furnace, which provides a more controllable condition in our growth experiments. 0.015 g of sulfur powder (>99.95%, Sigma Aldrich) was placed in zone 1 in a corundum groove, upstream. 0.5 g of WO_3 powder (>99. 5%, Sigma Aldrich) was uniformly spread on a quartz holder in zone 2, downstream, 14 cm away from the sulfur powder. A Si wafer with a thickness of 300 nm SiO_2 coated was placed upside down, 5 mm right above the WO_3 powder. The substrate was treated through the sonication in acetone, IPA and DI water for 10 minutes, respectively. The system was vacuumed for 30 minutes, then refilled with Argon and H_2 (3%) mixed gas. The WO_3 powder was heated to 880 ^oC at a rate of 15^0C/min, in the meanwhile the sulfur powder was heated to 250 ^oC. Then zone 2 was slowly cooled down to 780 ^oC in 40 minutes, and zone 1 was hold at 250 ^oC. Subsequently, the whole system started to cool down to room temperature naturally. Argon and H_2 (3%) mixed gas was flowed with a flowing rate of 50 sccm during the whole growth process. Schematic diagrams of the APCVD system we set up for the experiments and the temperature ramp was shown in figure S1 (a) and (b). All Raman and PL spectra here were obtained with a laser of 532 nm (2.33 eV) as excitation source. Only one parameter was changed in every single experiment, compared with the best growth condition we introduced above.

Results and discussion

As we know, H_2 is more reductive than sulfur. The reduction activity of WO_3 could be promoted with the participation of H_2 gas,[34] leading to high concentration of WO_{3-x} by the reaction between H_2 and WO_3. The necessity of H_2 was confirmed in our experiment. Without H_2 gas flow, we found there was no reaction happened in WO_3 powder during the whole process. In addition it has been reported that too high concentration of H_2 could restrain the size of WS_2 domains to enlarge.[34] We chose 3% H_2 mixed with argon as carrier gas, in consideration of both reaction kinetics and dimension control.

Temperature issue is also well-considered during our synthesis experiments. At a higher growth temperature it causes negative effects on nucleation and deposition process, mainly due to the enhancement of diffusion rate and decline of crystal stability at higher temperature. On the other hand, higher growth temperature offers higher energy in thermodynamics, promoting the reaction of WO_3/WO_{3-x} and sulfur vapor, as well as crystal quality of as-grown monolayer WS_2. Therefore, we employed a slowly cooling down process in the growth as described in experimental details to improve both growth quality and coverage.

Figure 1a exhibits the optical image of an isolated and clean CVD-grown WS_2 monolayer on SiO_2/Si substrate with a size of ~ 52 μm. The optical image (Figure S1(c), Supporting Information) also exhibits the large-area growth of WS_2 triangular domains. The fine triangular shape with clean surface and smooth edge indicates the

high quality of our as-grown WS_2 triangular. Furthermore, the thickness of the as-synthesized WS_2 domain was ~ 0.83 nm measured by AFM as demonstrated in the height profile shown in the inset of figure 1b. The HRSTEM characterization of monolayer WS_2 was shown in Figure 1c. The hexagonal rings of alternative W and S atoms in each unit are denoted by blue and yellow spheres representing W atoms and S atoms, respectively. It indicates defect-free atomic lattices of our as-grown WS_2 monolayer. The corresponding selected area electron diffraction (SAED) pattern with [001] zone axis (the inset of Figure 1c) revealed the single crystalline nature of our as-grown monolayer WS_2.

Raman spectrum plays a key role to identify the number of layers in as-grown WS_2 domains.[35] The strongest peak at ~350 cm^{-1}, according to the calculated phonon dispersion[36] and experimental studies,[29] comprises an in-plane vibration of $E^1_{2g}(\mathrm{M})$ mode, a second-order mode of longitudinal acoustic phonon $2\mathrm{LA(M)}$ mode and an in-plane vibration of $E^1_{2g}(\Gamma)$ mode. It was resolved by multi-peak Lorentzian fitting as shown in Figure 2a. (Table S1, Supporting Information). The out-of-plane $A_{1g}(\Gamma)$ mode peak at ~419 cm^{-1}, the combination modes of $2LA - 2E^2_{2g}$ peaks at ~300 cm^{-1} and ~323 cm^{-1} were also labeled in Figure 2a. A frequency separation of ~ 62 cm^{-1} between $E^1_{2g}(\Gamma)$ and $A_{1g}(\Gamma)$ has been treated as the spectral finger print of WS_2 monolayer,[35] which confirms the monolayer configuration of as-synthesized WS_2.

A Photoluminescence (PL) peak (Figure 2b) was observed at 630.4 nm (1.97 eV) in the as-synthesized monolayer WS_2 at room temperature, which mainly originates from A-exciton emission. It is the direct excitonic transition between the lowest

conduction band (CB) and the highest valence band (VB) at the same K point in the Brillouin zone.[30, 36] The PL peak location is consistent with our DFT-GGA band gap calculation (1.81 eV), as shown in Figure 2c. The full-width at half-maximum (FWHM) of ~15 nm also conforms to previous studies.[37] Particularly, we studied the frequency shifts of $E^1_{2g}(\Gamma)$ and $A_{1g}(\Gamma)$ peaks and the PL peak shift induced by different thickness in a mixed layer-number WS_2 flake (Figure S2, Supporting Information). With an increase of layer numbers, a slight red-shift of $E^1_{2g}(\Gamma)$ peak can be observed, while $A_{1g}(\Gamma)$ peak exhibited larger blue-shift. The increase of number of layers strongly enhances the out-of-plane vibrations, while Coulomb interactions tend to decrease the frequency of the in-plane vibrations, leading to monotonous increase in frequency separation between $E^1_{2g}(\Gamma)$ and $A_{1g}(\Gamma)$ peaks.[32, 33, 36] The intensity of the PL peak rapidly drops with an increase in the number of layers, which is corresponding to a band transition from direct to indirect band gap in WS_2.

In order to have a better understanding of the growth mechanism, a series of experiments were conducted to investigate the impacts of experimental parameters. Temperature issue is an important growth parameter to achieve monolayer WS_2 triangular domains. We conducted a series of growth experiments by varying the furnace zone 2 temperature set point of 750 ^oC, 850 ^oC, 900 ^oC and 950 ^oC, respectively. In the meanwhile the other growth parameters were fixed as the same. At 750 ^oC, there was no monolayer WS_2 growth achieved, instead only thick and aggregated WS_2 particles were observed on the substrate as shown in the Figure 3a.

The Raman spectrum in the inset of Figure 3a indicated a multilayer growth of WS_2 at the highlighted area by the red spot. The low temperature issue caused low diffusion rate of the precursor, which can easily leads to the precursor trapped at pre-growth sites on the substrate. As long as the very early precursor nucleation stage was reached, the nucleation sites were turned into trap centers and the subsequent precursor nucleated at those trapping sites. As a result, the thick and stacking morphology of WS_2 were obtained. With an increase of the temperature to 850 ^oC, monolayer WS_2 triangular domains with a size of ~ 30 μm were obtained as shown in Figure 3b. As the temperature increased to 900 ^oC, there is no big difference in the growth morphology compared to 850 ^oC, as shown in figure 3c. However, at 950 ^oC, no triangular domains can be grown as shown in the Figure 3d. To probe the reason of non-growth at 950 ^oC, we prepared a SiO_2/Si substrate coated with as-synthesized WS_2 monolayer. We loaded it in the tube furnace and heated up to 950 ^oC. Optical images were taken before and after the experiment at same spots (Figure S3). Almost all triangular WS_2 domains on the wafer disappeared after the heating process, and only few fragmentary remained. This experiment result illustrates the instability of triangular WS_2 domains under temperature of 950 ^oC, indicating the low thermo-stability of WS_2 is an important reason for non-growth beyond 950 ^oC. Generally, the higher temperature induces high diffusion rate of the precursor, which raises the possibility for the monolayer growth. On the other hand, too high temperature induces large thermal turbulence, as well as the instability of

as-synthesized WS_2 monolayer. It causes the growth hard to achieve stable nuclei at the beginning of the growth, which hinders the WS_2 growth.

The gas flow rate is another important growth parameter, which could be considered as the key of exposure time and S source controlling. At a gas flow rate lower than 5 sccm, there was no obvious growth observed resulting from less precursor transported to the growth substrate. Most sulfur vapor directly coagulated at upstream side of the heating zone instead of reacting with WO_3, leaving a thick layer of concretionary sulfur particle at the inside surface of the quartz tube at upstream side. The lack of sulfur vapor in the reaction led to exorbitant concentration of WO_3/WO_{3-x}, leading to the impurity deposition on substrate (Figure S5, Supporting Information), increase of thickness and irregular growth in shape. The impurity is probably due to the existence of intermediates of sulfuretted tungsten.[28] Slightly increase the gas flow rate, extensive nucleation was observed at 10 sccm as shown in Figure 4a. Lower gas flow rate causes in longer exposure time resulting in extensive nucleation. With an increase of gas flow rate, more precursor can be flowed to the substrate, providing S source for nucleation and growth. The representative image of WS_2 hexagonal domains grown at flow rate of 15 sccm was demonstrated in Figure 4b. As indicated, three side lengths of the hexagon were shorter than the other three side lengths (Figure 4b), which could be due to the different growth velocities beginning from the same nucleus.[38] Presumably this hexagonal configuration is an early stage in growth of monolayer WS_2 triangular domains. On account of the differences in the velocities of growth of the different side lengths, the hexagonal

shape would, on growing, approximate more and more to a triangular shape.[38] When gas flow rate reaching to 20 sccm, enough precursor can be transferred to the substrate. Three longer side lengths intersect with each other and the shorter side lengths disappear. As a result, it turns the hexagon shape into a triangular domain configuration. The as-grown monolayer WS_2 has an average domain size of ~ 25 μm at 20 sccm. Continuously raising the gas flow rate, the monolayer WS_2 domains increased in size. At a gas flow rate of 50 sccm, the triangular domain size reached an average value of ~ 45 μm. As the gas flow rate raised beyond value of 50 sccm, the triangular domain size started to decrease. At a gas flow rate of 80 sccm, it decreased to ~10 μm in average. The typical optical images of triangular domains grown under different flow rate and the plot of the domain size versus gas flow rate are demonstrated in Figure 4c. As the gas flow rate reached the point of 150 sccm, there was no domain growth observed on the substrate (Figure S4, Supporting Information). Because of too high gas flow rate, too much precursor was transferred to the downstream side of the tube end instead of the growth substrate. Another interesting comet-like growth morphology was observed at a gas flow rate of 100 sccm as shown in Figure 4d. The "head" region and the "tail" region were circled in yellow line and black line, respectively. Raman spectra (Figure S6, supporting information) confirmed that both the "head" and the "tail" of the "comet" were consisted of WS_2 multi-layer triangular domains. Compared to "head", there is a red shift of A_{1g} mode observed in "tail" with $\Delta\omega$=2 cm-1, and for E_{2g}^1 mode, a blue shift ($\Delta\omega$=1 cm-1) observed in "tail". It indicates that the "tail" has less number of layers than the "head".[39] A

possible explanation is that the higher gas flow rate generated drastic turbulence around the growth substrate surface, which broke up early-formed nucleation sites and causes a trace formation along the gas flow orientation. It comes to a conclusion that gas flow rate determines the exposure time and the amount of S source participating in the reaction, exerting important impact on the precursor nucleation and nucleus growth.

Conclusion

We have demonstrated the synthesis of high quality and large-area monolayer WS_2 triangular domains on SiO_2/Si substrate by APCVD method. The growth parameters including gas flow rate, growth temperature and precursor ratio have been optimized by a series of systematical investigations. A growth mechanism was proposed based on the fundamental analysis. Our results provide some general guidelines for other 2D monolayer synthesis of TMD.

Acknowledgements

This work was supported by National Natural Science Foundation of China (NSFC) (21373196), the Recruitment Program of Global Experts, the Fundamental Research Funds for the Central Universities (WK2060140014, WK2340000050).

References

1. A. K. Geim and K. S. Novoselov, *Nat. Mater.*, 2007, **6**, 183.
2. A. K. Geim, *Science*, 2009, **324**, 1530.

3. K. S. Novoselov, *Rev. Mod. Phys.*, 2011, **83**, 837.

4. J. van den Brink, *Nat. Mater.*, 2010, **9**, 291.

5. A. H. C. Neto and K. S. Novoselov, *Rep. Prog. Phys.*, 2011, **74**, 82501.

6. M. Xu, T. Liang, M. Shi and H. Chen, *Chem. Rev.*, 2013, **113**, 3766.

7. Q. Wang, K. Kalantar-Zadeh, A. Kis, J. N. Coleman and M. S. Strano, *Nat. Nanotechnology*, 2012, **7**, 699.

8. M. Chhowalla, H. Shin, G. Eda, L. Li, K. P. Loh and H. Zhang, *Nat. Chem.*, 2013, **5**, 263.

9. X. Huang, Z. Zeng and H. Zhang, *Chem. Soc. Rev.*, 2013, **42**, 1934.

10. S. Z. Butler, S. M. Hollen, L. Cao, Y. Cui, J. A. Gupta, H. R. Gutierrez, T. F. Heinz, S. Hong, J. Huang, A. F. Ismach, E. Johnston-Halperin, M. Kuno, V. V. Plashnitsa, R. D. Robinson, R. S. Ruoff, S. Salahuddin and J. Shan, *ACS Nano*, 2013, **7**, 2898.

11. H. S. S. R. Matte, A. Gomathi, A. K. Manna, D. J. Late, R. Datta, S. K. Pati and C. N. R. Rao, *Chem. Int. Ed.*, 2010, **49**, 4059.

12. K. F. Mak, C. Lee, J. Hone, J. Shan and T. F. Heinz, *Phys. Rev. Lett.*, 2010, **105**, 136805.

13. W. Zhao, Z. Ghorannevis, L. Chu, M. Toh, C. Kloc, P. Tan and G. Eda, *ACS Nano*, 2013, **7**, 791.

14. Y. Li, L. Li, Carlos Moyses Araujp, L. Wei and Rajeev Ahuja, *Catal. Sci. Technol.*, 2013, **3**, 2214.

15. Y. H. Lee, X. Zhang, W. Zhang, M. Cheng, C. Lin, K. Chang, Y. Yu, J. Wang, C.

Chang, L. Li and T. Lin, *Adv. Mater.*, 2012, **24**, 2320.

16. S. Wu, C. Huang, G. Aivazian, J. S. Ross, D. H. Cobden and X. Xu, *ACS Nano*, 2013, **7**, 2768.

17. S. Najmaei, Z. Liu, W. Zhou, X. Zou, G. Shi, S. Lei, I. Boris, Yakobson, Idrobo J-C, P. M. Ajayan and J. Lou, *Nat. Mater.*, 2013, **12**, 754.

18. K. Liu, W. Zhang, Y. H. Lee, Y. Lin, M. Chang, C. Su, C. Chang, H. Li, Y. Shi, H. Zhang, C. Lai and L. Li, *Nano Lett.*, 2012, **12**, 1538.

19. A. Splendiani, L. Sun, Y. Zhang, T. Li, J. Kim, C-Y Chim, G. Galli and F. Wang, *Nano Lett.*, 2010, **10**, 1271.

20. A. M. van der Zande, P. Huang, D. A. Chenet, T. C. Berkelbach, Y. You, G. H. Lee, T. F. Heinz, D. R. Reichman, D. A. Muller and J. C. Hone, *Nat. Mater.*, 2013, **12**, 554.

21. D. J. Late, B. Liu, H. S. S. R. Matte, V. P. Dravid and C. N. R. Rao, *ACS Nano*, 2012, **6**, 563.

22. D. Jariwala, V. K. Sangwan, D. J. Late, J. E. Johns, V. P. Dravid, T. J. Marks, L. J. Lauhon and M. C. Hersam, *Appl. Phys. Lett.*, 2013, **102**, 173107.

23. T. Cao, G. Wang, W. Han, H. Ye, C. Zhu, J. Shi, Q. Niu, P. Tan, E. Wang, B. Liu and J. Feng, *Nat. Commun.*, 2012, **3**, 887.

24. D. Xiao, G. Liu, W. Feng, X. Xu and W. Yao, *Phys. Rev. Lett.*,2012, **108**, 196802;

25. Y. Wang, C. Cong, C. Qiu and T. Yu, *Small*, 2013, **9**, 2857.

26. C. Rice, R. J. Young, R. Zan, U. Bangert, D. Wolverson, T. Georgiou, R. Jalil

and K. S. Novoselov, *Phys. Rev. B*, 2013, **87**, 081307.

27. W. J. Schutte, J. L. Deboer and F. Jellinek, *J. Solid State Chem.*, 1987, **70**, 207.

28. C. Cong, J. Shang, X. Wu, B. Cao, N. Peimyoo, C. Qiu, L. Sun and T. Yu, *Adv. Optical Mater.*, 2014, **2**, 131.

29. H. Zeng, G. Liu, J. Dai, Y. Yan, B. Zhu, R. He, L. Xie, S. Xu, X. Chen and W. Yao, *Sci. Rep.*, 2013, **3**, 1608.

30. N. Perea-López, A. L. Elías, A. Berkdemir, A. Castro-Beltran, H. R. Gutiérrez, S. Feng, R. Lv, T. Hayashi, F. López-Urías, S. Ghosh, B. Muchharla, S. Talapatra, H. Terrones and M. Terrones, *Adv. Funct. Mater.*, 2013, **23**, 5511.

31. D. Voiry, H. Yamaguchi, J. Li, R. Silva, D. C. Alves, T. Fujita, M. Chen, T. Asefa, V. Shenoy and G. Eda, *Nat. Mater.*, 2013, **12**, 850.

32. Y. H. Lee, L. Yu, H. Wang, W. Fang, X. Ling, Y. Shi, C. Lin , J. Huang, M. Chang and C. Chang, *Nano Lett.*, 2013, **13**, 1852.

33. H. R. Gutierrez, N. Perea-Lopez, A. L. Elias, A. Berkdemir, B. Wang, R. Lv, F. Lopez-Urias, V. H. Crespi, H. Terrones and M. Terrones, *Nano Lett.*, 2012, **13**, 3447.

34. Y. Zhang, Y. Zhang, Q. Ji, J. Ju, H. Yuan, J. Shi, T. Gao, D. Ma, M. Liu, Y. Chen, X. Song, H. Y. Hwang, Y. Cui and Z. Liu, *ACS Nano*, 2013, **7**, 8963.

35. A. Berkdemir, H. R. Gutierrez, A. R. Botello-Mendez, N. P. Lopez, A. L. Elias, C. I. Chia, B. Wang, V. H. Crespi, F. Lopez-Urias, J. C. Charlier, H. Terrones and M. Terrones, *Sci. Rep.*, 2013, **3**, 1755.

36. A. Molina-Sanchez and L. Wirtz, *Phys. Rev. B*, 2011, **84**, 155413.

37. Y. Rong, Y. Fan, K. A. Leen, A. W. Robertson, K. He, S. Wang, H. Tan, R. Sinclair and J. H. Warner, *Nanoscale*, 2014, **6**, 12096.

38. T. Michely, M. Hohage, M. Bott and G. Comsa, *Phys. Rev. Lett.*, 1993, **71**, 1659.

39. N. Peimyoo, J. Shang, C. Cong, X. Shen, X. Wu, E. K. L. Yeow and T. Yu, *ACS Nano*, 2013, **7**, 10985.

Figure captions

Figure 1. (a) Optical image of monolayer WS_2 triangular domain with a side length of ~ 52 μm. (b) AFM image of as-grown monolayer WS_2 triangular domain. The line profile in the inset indicates the WS_2 monolayer is ~ 0.83 nm thick. (c) HRSTEM image indicates defect-free atomic lattices of our as-grown WS_2 monolayer. The inset blue and yellow cartoon atoms represent the W and S atoms, respectively. The electron diffraction pattern in the inset indicates single crystalline structure. The zone axis is along [001] direction.

Figure 2. (a) Raman spectrum of the as-grown monolayer WS_2. The Raman modes are analyzed by multi-peak Lorentzian fitting. (b) PL spectrum of as-grown monolayer WS_2 with an emission peak observed at 630.4 nm (1.97 eV) excited by 532 nm laser. (c) Calculated band structure of monolayer WS_2 with a band gap of 1.81 eV.

Figure 3. Optical images of WS_2 growth grown at (a) 750 ^oC, (b) 850 ^oC, (c) 900 ^oC and (d) 950 ^oC with the same flow rate of 50 sccm. The Raman spectrum in the inset of (a) indicates a multilayer growth of WS_2. The red dot in (a) represents the laser spot location. Monolayer WS_2 triangular domains can be achieved in a range from 850 ^oC to 900 ^oC.

Figure 4. 0.015 g of sulfur powder and 0.5 g of WO_3 powder were loaded. The sulfur powder was heated to 250 ^oC and the WO_3 powder was heated to 880 ^oC at 15 ^oC/min. (a) Optical image of growth result grown at gas flow rate of 10 sccm. (b) Optical image of a WS_2 hexagonal domain obtained at gas flow rate of 15 sccm. (c) Statistical analysis of domain size influenced by different gas flow rate. Error bar shown in red.

Inset is the representative optical images of monolayer WS_2 domains grown at flow rate of 20, 50 and 80 sccm, respectively. Scale bar is 10 μm. (d) Optical image of comet-like WS_2 domains. The "head" and the "tail" regions are labeled by yellow and black circles, respectively. Inset is the high magnification image of the "tail".

Figures

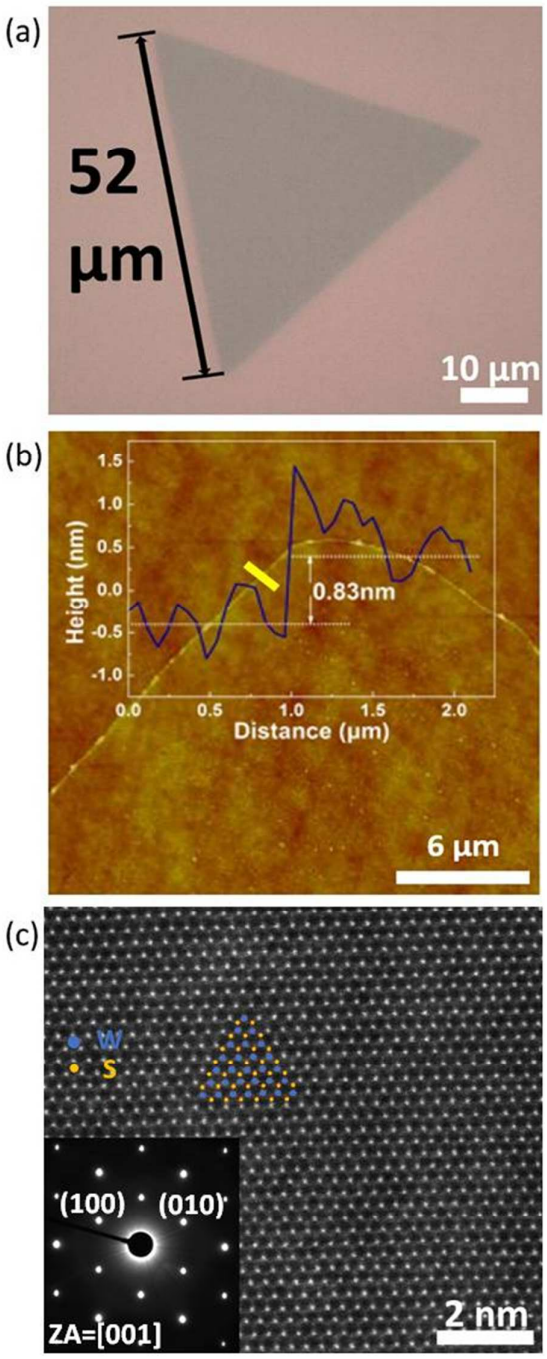

Figure 1

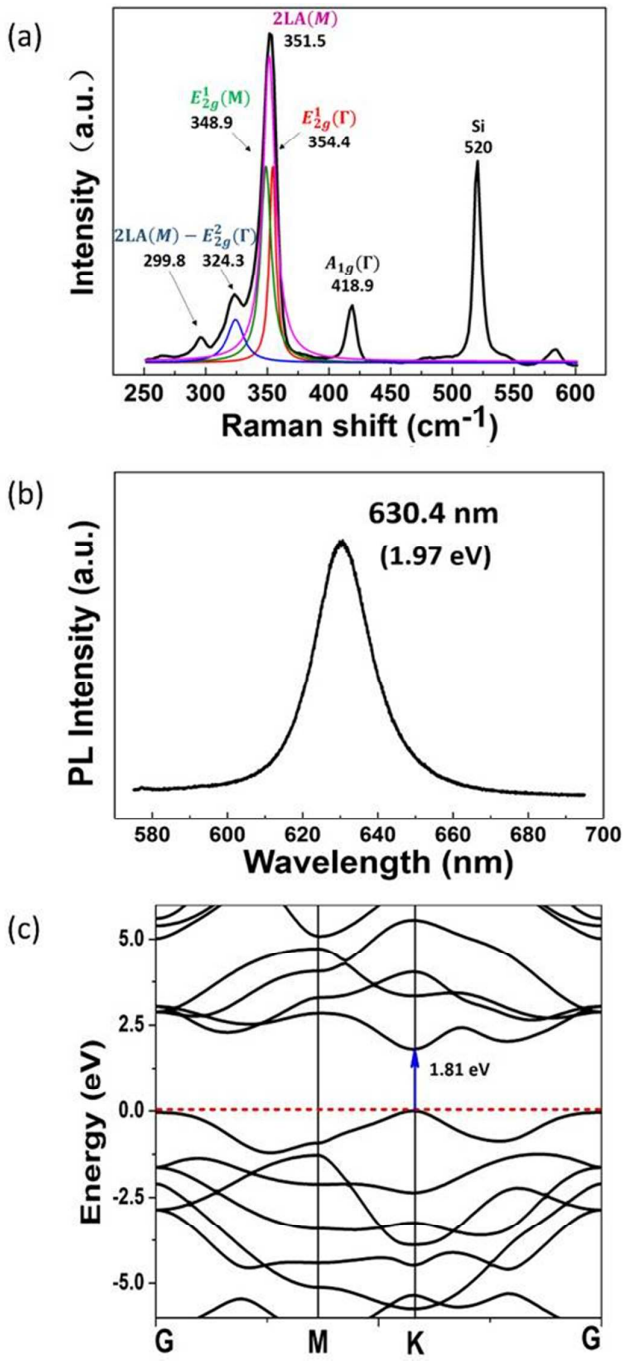

Figure 2

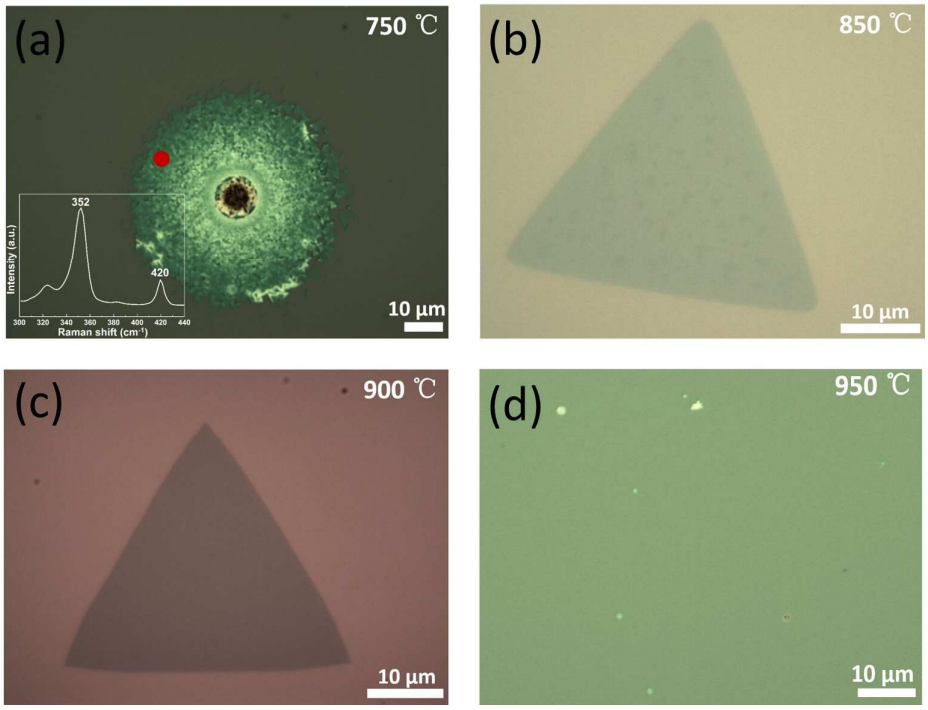

Figure 3

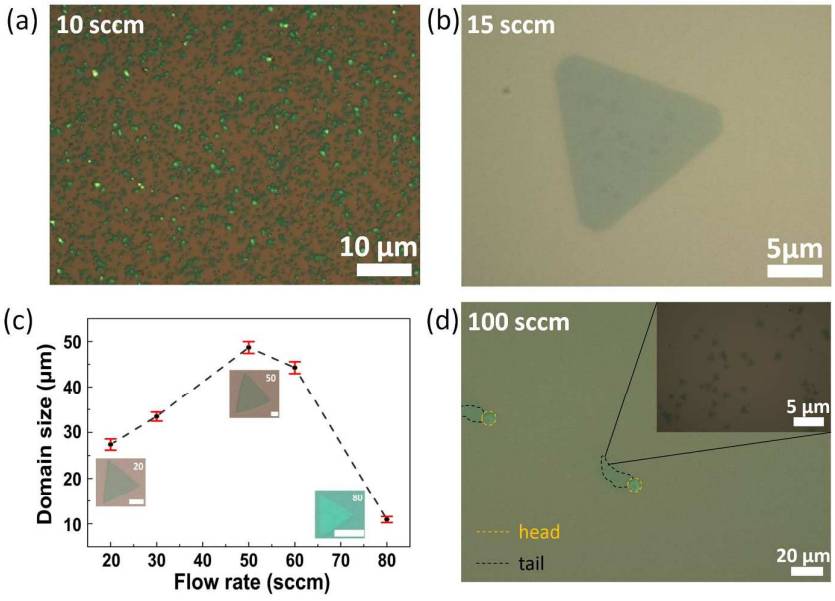

Figure 4